G04p-92/035

GSI

GSI-92-27
PREPRINT
APRIL 1992

MULTIPLICITY AND PSEUDORAPIDITY DISTRIBUTIONS OF CHARGED PARTICLES FROM ^{32}S INDUCED HEAVY ION INTERACTIONS AT 200 A GeV

WA 80 COLLABORATION
R. ALBRECHT et al.

(Submitted to Z. Phys. C)

Gesellschaft für Schwerionenforschung mbH
Planckstr. 1 · Postfach 11 05 52 D-6100 Darmstadt 11 · Germany

MULTIPLICITY AND PSEUDORAPIDITY DISTRIBUTIONS OF CHARGED PARTICLES FROM ^{32}S INDUCED HEAVY ION INTERACTIONS AT 200 A GeV

WA80 Collaboration

R Albrecht[1], T C Awes[2], C Baktash[2], P Beckmann[3], F Berger[3], M A Bloomer[4], D Bock[3], R Bock[1], G Claesson[5], G Clewing[3], L Dragon[3], A Eklund[5], R Ferguson[2], A Franz[6], S I A Garpman[5], R Glasow[3], H-Å Gustafsson[5], H H Gutbrod[1], G Hoelker[3], J Idh[5], P Jacobs[4], K-H Kampert[3], B W Kolb[1], H Löhner[7], I Lund[7], F E Obenshain[2,6], A Oskarsson[5], I Otterlund[5], T Peitzmann[3], F Plasil[2], A M Poskanzer[4], M L Purschke[1], H-G Ritter[4], B Roters[1], S Saini[2], R Santo[3], H R Schmidt[1], S P Sorensen[2,6], P Steinhaeuser[1], K Steffens[3], E Stenlund[5], D Stüken[3] and G R Young[2]

Abstract

Multiplicity and pseudorapidity distributions have been measured for ^{32}S + Al, Cu, Ag and Au at 200 A GeV. The widths of the pseudorapidity distributions increase from central to peripheral collisions. The main contribution is explained by the increasing fraction of charged particles stemming from the fragmentation of the target for peripheral collisions as compared to central collisions. On the average 170–180 charged particles per unit of pseudorapidity are attained for the most central ^{32}S+Au events. The target dependence of the yield of charged particles for central collisions is investigated. In the target rapidity region the yield is directly proportional to the target mass. The transverse energy per charged particle has been studied as a function of centrality and pseudorapidity. The experimental results are compared to the results from the Monte–Carlo model VENUS 3.11 which includes rescattering among secondaries. A comparison between different centrality triggers is made.

(Submitted to Z. Phys. C.)

[1]Gesellschaft für Schwerionenforschung (GSI), Planckstr 1, Postfach 110541, D-6100 Darmstadt, Germany

[2]Oak Ridge National Laboratory (ORNL), POB 2008, Oak Ridge, TN 37831-6372, USA

[3]Inst für Kernphysik, University of Münster, Wilhelm-Klemm Str. 9, D-4400 Münster, Germany

[4]Nuclear Science Division, Lawrence Berkeley Laboratory, Berkeley, CA 94720, USA

[5]Division of Cosmic and Subatomic Physics, Dept of Physics, University of Lund, Sölvegatan 14, S-223 62 Lund, Sweden

[6]University of Tennessee, Knoxville, TN 37996-1200, USA

[7]KVI, University of Groningen, NL-9747 AA Groningen, The Netherlands

1 Introduction

Multiplicity and pseudorapidity distributions of charged particles from heavy ion interactions at ultrarelativistic energies give information on the geometry and dynamics of nuclear interactions. The establishment of a phase transition from normal nuclear matter to a quark–gluon plasma[1] is the main goal in the study of high energy nuclear collisions. One of the prerequisites for a plasma formation is a high enough energy density. The energy density can be estimated from the measured charged particle or transverse energy densities[2].

Multiplicity measurements at relativistic energies have been performed by several experiments using a variety of detectors: emulsion, streamer tube arrays, silicon pad arrays and streamer chambers. At Brookhaven multiplicity and rapidity measurements have been performed with 14.6 A GeV ^{28}Si on various targets [3, 4, 5, 6]. From CERN there have been similar results for 60 and 200 A GeV ^{16}O projectiles[5, 6, 7, 8, 9] and 200 A GeV ^{32}S projectiles [10, 11, 12, 13, 14].

This paper presents multiplicity and pseudorapidity distributions for ^{32}S on Al, Cu, Ag and Au targets at 200 A GeV. The data were taken with the WA80–setup[15] at CERN. Comparisons are made with some of the results from other experiments and with the VENUS model[16] version 3.11.

2 Experimental Setup

The detectors employed in the analysis presented in this paper have been described in detail elsewhere[17, 18, 19, 20]. In the following follows a brief description of the relevant WA80 detectors.

2.1 The Plastic Ball

The Plastic Ball[17] is made of 655 ΔE–E scintillator telescopes surrounding the target. The particle identification possibilities are not used in this analysis.

The Plastic Ball covers the pseudorapidity interval -1.7$< \eta <$1.4, where η is defined as η = -ln(tan($\frac{\theta}{2}$)). θ is the polar angle with respect to the beam. The azimuthal coverage in the region 1.2$< \eta <$1.4 is only partial and in this region the Plastic Ball overlaps with the streamer tube detectors.

2.2 The Streamer Tube Detectors

Four planes of Iarrocci–type streamer tubes[18] with pad read–out form the WA80 streamer tube detectors. The planes are placed together two and two to obtain double coverage for all angles. The Large Angle Multiplicity detector (LAM) consists of two planes, LAM1 and LAM2 placed 227 cm and 268 cm downstream from the target, respectively. They cover the region 1.2$< \eta <$3.0. The Midrapidity Multiplicity detector (MIRAM) consists of two planes, MIRAM1 and MIRAM2 at

the distances 501 cm and 549 cm from the target, respectively. They have coverage in the interval 2.6< η <4.2. In the region 2.6< η <3.0 both LAM and MIRAM are used to obtain complete azimuthal coverage.

The read–out of the planes is made by means of pads capacitively coupled to the streamer tubes. When a charged particle traverses a tube a discharge is produced which is sensed by the pad. If the signal exceeds a preset discriminator level the pad is signalled as "fired". Only the "fired" pads are read out for each event. The pads are placed on boards of the size 21x21 cm^2 equipped with comparators and electronics for serial read–out. The pads vary in size from 5.2x3.5 to 2.6x1.0 cm^2. The smallest pads are used in the innermost part of LAM and in the whole area of MIRAM to ensure the highest resolution where the particle density is the highest. A total of 43000 pads are used in the four planes.

2.3 The Zero Degree Calorimeter (ZDC)

The ZDC[19] is a compensated beam calorimeter placed 11 m downstream from the target. The coverage is $\theta < 0.3^o$ corresponding to $\eta > 6.0$. It is made of uranium sheets interleaved with plastic scintillators. The energy response to heavy ions is linear over the range 60–6400 GeV. The hadronic in–beam resolution varies from σ/E=0.013+0.33/$\sqrt{E/GeV}$ at low beam intensities (< 10^5 ions/s incident) to σ/E=0.02+0.67/$\sqrt{E/GeV}$ at higher beam intensities (10^6 ions/s incident).

The ZDC is used in the WA80 minimum bias trigger condition. An event is accepted as a minimum bias event if less than 88% of the beam energy is measured in the ZDC and at least one charged particle is recorded in either LAM or MIRAM. In the analysis we require less than 85% of the beam energy in the ZDC.

2.4 The Midrapidity Calorimeter (MIRAC)

The transverse energy, E_T, of the interaction is measured by the calorimeter MIRAC[20]. It has full coverage for the region 2.4< η <5.5 and partial coverage out to η=1.6. The response of the calorimeter is measured to be linear over the energy range of 2 to 50 GeV. It has a lead–scintillator electromagnetic section and an iron–scintillator hadronic section. The energy resolution of the electromagnetic section was σ/E=0.014+0.11/$\sqrt{E/GeV}$ and for the hadronic section σ/E=0.034+0.34/$\sqrt{E/GeV}$.

3 Data Analysis

Several background corrections are applied to the data. The background comes both from real particles and from noise in the electronics and detectors. Real particles may be produced in secondary interactions with the materials of the setup but can also come from the beam halo, albedo neutrons from the calorimeters and

from cosmic rays. Sparking in the streamer tubes as well as electronic noise may give rise to unintentionally fired pads.

First a pad rejection is made. The fired pads of LAM2 are projected onto LAM1 assuming the centre of the target as the vertex. Pads in either LAM1 or LAM2 which do not geometrically overlap with pads in the other plane are rejected and not used in the analysis. The procedure is similarly applied to the fired pads of MIRAM2 which are projected on to MIRAM1. The second step is to connect neighbouring pads to form clusters. Clusters containing more than four pads are usually produced by more than one particle[18]. These clusters are split in two, or if they are big, sometimes even three or four smaller clusters. Clusters containing more than ten pads are not split due to the lack of information on how they should be divided. These large clusters are very unusual, 0.2–0.3% of the total number of clusters. These remaining clusters now form the hits in one plane and the hit position is calculated as the center of gravity of the pads contained in the pattern, equally weighted. The third step is to correlate planes to determine which hits in the two planes are associated with the same track. One pad in one plane may overlap with two pads in the second plane which are not connected.

3.1 Detection Probabilities

The streamer tube detectors do not have 100% detection probability for charged particles. Each streamer tube consists of 8 subcells. Between the subcells there is a thin wall about 1 mm wide. Particles that strike the streamer tubes in these walls instead of in the gas filled subcells will not produce any ionization in the gas. These particles will not give rise to any discharge and hence not be sensed by the pads. The side walls of the streamer tubes are somewhat thicker than the walls between the subcells. The geometry of the setup was used as input in a Monte–Carlo simulation to determine the acceptance. The streamer tubes are oriented vertically, therefore the acceptance increases for large angles left and right but varies hardly at all up and down. The acceptance for perpendicular tracks is about 89% and for large horizontal angles ($\approx 30°$) about 98%. In addition to this purely geometrical effect of the streamer tubes there is an additional inefficiency of the pads. Between the pads are thin insensitive regions, which may account for some losses of charged particles. A too high discriminator level can also give rise to some losses. The board detection probability, i.e the total probability that a particle that produces a streamer in the streamer tubes will be sensed by at least one pad, was found to be about 93%. This has to be multiplied with the above angle dependent tube acceptance to give the total detection probability of the streamer tube detectors for charged particles.

3.2 Multiple Hit Corrections

We will refer to the probability that two or more particles will hit the same detector module, and be counted as one, as the multihit probability of that module. For the

streamer tube detectors the multihit probability is simulated with model events having the same multiplicity as the real events. Tracks are generated randomly with the same angular distribution as the real events and pads lying along their trajectory are fired according to the detection probabilities above. A pad response similar to that observed in the data is used. The fired pads are then fed through the same analysis program as the real events. At η=3.5 the correction factor is at most 1.5 in high multiplicity events and it reaches 2.0 at η=3.9. The analysis has been restricted to η <4.0.

In the forward region of the Plastic Ball the multihit corrections are also large in high multiplicity events. 60–70% of the modules in the most forward part of the detector are hit in the events with the highest multiplicities.

To correct for multihit in the Plastic Ball a different method than the one used for the streamer tube detectors has been employed for the pseudorapidity distributions. It has been assumed that the number of particles hitting a detector module are distributed according to Poisson statistics for a special event class. The event classes are defined by the energy measured at zero degrees. For Poisson statistics the probability to have zero particles in a module determines the mean, m, and thereby the whole distribution. Every hit detector module is therefore weighted with a factor $m/(1-e^{-m})$ to extract the mean number of particles per event for that event class. m depends on the event class as well as the size and position of the module. The denominator, $1-e^{-m}$, is the probability that a module is hit by at least one particle.

The method cannot be used event–by–event, but only as an average correction for a special event class with events that have the same multiplicity. An event class defined by the energy measured at zero degrees does not contain events with a fixed multiplicity, not even for a very narrow energy interval. This gives a systematic error to this method. This type of correction has been used previously[4, 7].

The method using Poisson statistics causes problems when we want to study multiplicity distributions. Since the Poisson method cannot be used event–by–event a different method to correct for multihit effects has to be used to get out a correct multiplicity distribution. For the multiplicity distribution in the Plastic Ball region a similar multihit method to the one used for the streamer tube detectors was employed. This method underestimates systematically the yield in the most forward region of the Plastic Ball compared to the Poisson method. The difference is about 15% for the events with the highest multiplicity. The total multiplicity in these events is underestimated by about 1% due to this effect. For low multiplicity events both the methods give the same result. The multiplicity distributions have not been corrected for this small effect.

3.3 Secondary Interactions in the Detector Material

Particles produced in interactions reach the streamer tube detectors after passage through several material: 1. The target, 2. Either the Aluminium target chamber or a carbon fibre beam–pipe placed downstream, 3. Air, 4. The upstream detector

LAM to reach the downstream detector MIRAM.

Using the radiation lengths, interaction lengths and thicknesses of the materials of the setup both the probabilities for gamma conversion and for hadronic interactions were calculated. A parameterization of data compiled by Albini et al.[21] was used to obtain the average multiplicities of secondary particles as a function of the momentum of the primary particle.

The correction for gamma conversion is at most 4.7% at η=4.0. Electron-positron pairs produced by gamma conversion will have a small opening angle and in most cases both particles will hit the same pad.

The probability for hadronic interactions is low, only 1–3%, but since several secondary particles can be produced it is still an important correction. At small angles, η=4.0, the correction is about 7%, but decreases with increasing polar angle because of the decrease in average momentum of the primary particles.

To calculate the contribution to the charged particle yield coming from interactions in the target frame, an empty target run was made. The relative contribution is highest for high energies measured by the ZDC i.e. peripheral collisions, and is most important for the lightest target. It was not more than 0.2% over the η–region covered by the streamer tube detectors and did only exceed 1% at η <–1.0 with a maximum of 5% at η=–1.7. No correction of the data was done for the no target yields.

3.4 Comments on Systematic Errors

The statistical errors of the distributions of this paper are small compared to the systematic ones. Some of them are difficult to calculate and an estimate is based on the variations of the results when one attempts different methods and strategies. Below is a brief description of the sources of systematic errors and an estimate of the systematic errors on the total yield.

For the Plastic Ball the multihit correction is based on the assumption of independent particles. A correlation between particles would affect the multihit probability. It is believed to be a small effect and is not corrected for. Low energy particles, below 10 MeV, are absorbed in the target or the target chamber and are not detected. Also for the streamer tube detectors there is a low energy cutoff. A minimum kinetic energy of 25 MeV is needed for a proton to penetrate two detector planes deep enough to be detected by both of them. The corresponding threshold for charged pions is 14 MeV. In the region covered by the streamer tube detectors almost all particles are relativistic and the cutoff energy should not influence the yield significantly.

The accuracy of the hit correlation between planes is strongly multiplicity dependent and is naturally worst for the high multiplicity events. For low multiplicity the systematic error is estimated to 1%. For high multiplicity the hit correlation is of course strongly coupled to the multihit correction and they are expected to contribute 5% each to the systematic error. For η >3.5 where multihit effects are severe it may reach 10–15% totally.

The measurement of the streamer tube acceptance and the board efficiency are connected and the combined systematic error is set to 2%. It should not depend on the multiplicity of the event. Since only correlated hits are used the values for streamer tube acceptance and board efficiency appear squared in the correction. The total systematic error is therefore 4%.

The corrections from secondary interactions in the materials of the setup are at worst 11–12%. The systematic error in this case is dominated by the accuracy of the parameterization for the number of particles produced in hadronic interactions. The contribution to the systematic error should not exceed 2% of the total yield of particles.

To conclude, the combined systematic error to the total yield for low multiplicity events in the region covered by the streamer tubes is believed to be 4–5%. For high multiplicity events it is estimated to be 8–9%, except in the most forward region around η=4.0 where it may reach 15%. These total systematic errors have been obtained by quadratic addition of the different partial errors.

4 Results

The distributions presented in this paper have been obtained with statistics ranging from 33000 minimum bias events for the gold target to 52000 for the copper target. The minimum bias cut used in the off–line analysis is that less than 85% of the beam energy must be measured in the zero degree calorimeter. The targets were thin to keep γ conversion and multiple interactions to a minimum. The thickness was 250 mg/cm^2 for the gold target and 200 mg/cm^2 for the other targets. For each target 20000 events have been simulated using VENUS. The VENUS zero degree energy distribution is similar to the WA80 distribution and it should be possible to compare results for different trigger cuts.

4.1 Multiplicity Distributions

The multiplicity distributions for charged particles in ^{32}S + Al, Cu, Ag and Au interactions are shown in figure 1. The angular coverage is -1.7< η <4.0. As the thickness of nuclear matter to traverse increases the total multiplicity also increases.

The shape of the multiplicity distributions are dominated by geometry. There is a large probability for peripheral collisions, which have low multiplicity. The sudden drop at very low multiplicity is due to the trigger cut of 85% of the beam energy which removes most of the interactions with low multiplicity. The plateau stems from collisions with intermediate impact parameters. The knee at high multiplicity corresponds to the range of impact parameters, where all of the projectile overlaps with the target. The tail of the distribution is described by a Gaussian[22]. The error bars are only statistical. The solid lines are the results from VENUS. The VENUS cross section was calculated from its impact parameter distribution.

The agreement between the model and the experimental data is good.

4.2 Pseudorapidity Distributions

The pseudorapidity distributions of charged particles for ^{32}S + Al, Cu, Ag and Au interactions for various cuts in E_{ZDC} are shown in figure 2 to 5. The central cut corresponds to less than 20% of the beam energy in the ZDC. The intermediate cut is 45–55% and the peripheral cut is 75–85%. Since no events with E_{ZDC}/E_{beam} <20% exist for Al because of the small cross section the central cut for Al is chosen to be E_{ZDC}/E_{beam} <35%. Note the backward shift of the peak position with increasing centrality for the heavy targets. The shift is due to the fact that the ratio of target participants to projectile participants increases as the impact parameter decreases when the projectile is smaller than the target. The average centre-of-momentum rapidity is thereby moved backwards. The error bars include systematic and statistical errors. The statistical errors are negligible compared to the systematic errors.

The VENUS results are indicated with solid lines. The model overpredicts the maximum value for the central collisions and is slightly below for the peripheral. For Ag and Au the VENUS results are narrower and more forward peaked.

A Gaussian fit to the pseudorapidity distributions was made to extract the widths for different energy cuts in the ZDC. All the energy bins were 320 GeV wide. The η–interval used in the fit was 0.0–4.0. The three free parameters of the fit were the maximum value, ρ_{max}, the peak position, η_{peak}, and the width, σ. In figure 6 the ρ_{max} of the fit as a function of ZDC energy is shown for all four targets. A fit was also made to the VENUS data in the same η–interval as above. The VENUS results are indicated with the solid lines. In figures 6, 7 and 8 the error bars include the systematic errors due to the uncertainty in the absolute yield.

An extrapolation of the data in figure 6 towards E_{ZDC}/E_{beam}=1.0 gives ρ_{max}=0 for all targets. The value of 180 charged particles per unit of pseudorapidity for central collisions of ^{32}S+Au is used to estimate the attained energy density[2], ϵ, from (1).

$$\epsilon = \frac{3\rho_{max} m_T c}{2\tau_0 \pi R^2} \tag{1}$$

With m_T=0.37 GeV/c^2, τ_0=1 fm/c, R=1.2·A$^{1/3}$ fm and A=32 we arrive at ϵ=2.2 GeV/fm^3. The value calculated from the calorimetric measurements of WA80 was 2.0±0.1 GeV/fm^3[23].

The peak position of the Gaussian fits are shown in figure 7. As one goes to heavier and heavier targets the peak position moves backward for a constant value of E_{ZDC}. With increasing E_{ZDC} the peak position shifts backwards for Al, which is somewhat lighter than the projectile. For the three other targets, which are all heavier than the projectile, the peak position moves forward with increasing E_{ZDC}. The solid lines are, from the top of the figure, the VENUS results for Al, Cu, Ag and Au. VENUS shows the same trends, but the difference between the results for different targets is less pronounced than for the experimental data. For a central

collision of ^{32}S+Au the number of target participants was calculated to be 81. It was assumed that all of the gold nucleons within the path of the projectile were participants. All of the 32 projectile participants interacting with the 81 target participants gives a centre–of–momentum rapidity, y_{CM}=2.53.

The fitted width for all four targets is shown in figure 8. The solid lines are, from the top of the figure, the VENUS results for Au, Ag, Cu and Al. The width obtained from the experimental data increases with the size of the target and it decreases with increasing centrality. The dependence on centrality can be explained as follows. At 200 A GeV there is a substantial breakup of the target and projectile into nucleons, even for peripheral collisions. This means that in peripheral collisions a larger fraction of the charged particles stems from the fragmentation of target and projectile as compared to central collisions. The backward and forward regions are dominated by target and projectile fragmentation respectively, whereas the region around midrapidity is dominated by the produced particles. Since the yield of charged particles in the backward and forward regions does not increase as strongly with centrality as in the central region the widths decrease with centrality.

The behaviour of the width with centrality for VENUS is the same as for the WA80 data, but the effect is again less pronounced. The FRITIOF model[24] which does not include rescattering has a target independent and almost centrality independent width of 1.3–1.4, which agrees with the data only for the central collisions. The influence from rescattering was studied by looking at negative pions in VENUS events. The width of the π^- pseudorapidity distributions for ^{32}S+Au in VENUS show some centrality dependence. From about 1.3 to 1.5–1.6. It indicates that rescattering is responsible for part of the observed increase in width for peripheral collisions compared to central collisions.

The dependence of the width on target mass can be explained along the same lines as above. A heavy target has more spectator matter than a small target. The fragmentation of the target gives the largest contribution in the backward region and widens the pseudorapidity distribution. This is obvious when one compares figures 2 and 5 in the region $-1.0 < \eta < 1.0$. Also the rescattering is more pronounced for a large target.

The large error bars for the bins with the lowest value of E_{ZDC}/E_{beam} in figure 6, 7 and 8 depend on the low cross sections for these events.

4.3 Target Mass Dependence

The target mass dependence on the yield of charged particles as a function of pseudorapidity has been investigated for ^{16}O induced central collisions[9]. The same analysis is repeated here with sulphur as the projectile. The yield of charged particles is assumed to have a power–law dependence on the target mass number A, i.e. $\Delta n_{ch}/\Delta\eta \sim A^{\alpha}$. α is determined as a function of pseudorapidity. Central collisions are chosen with the cut $E_{ZDC}/E_{beam} < 0.20$. To extract α, the logarithm of the yield is plotted as a function of the mass number for the heavy targets Cu,

Ag and Au. A linear fit is made to the three data points and α is then given by the slope. Figure 9 shows how α varies with η. The solid line indicates the result from VENUS. For $\eta < 0$ α is constant and close to 1. For the ^{16}O data α only reached about 0.8 in the target rapidity region. A centrality cut of 20% of the beam energy corresponds on the average to smaller impact parameters for a sulphur projectile than for oxygen due to its larger size. The sulphur sample is therefore somewhat more central explaining the higher α–value. It is possible to interpret a value of α=1 as the whole target participating in the collison. Most of the particles in this region should however originate from the target spectators and it is not evident that they should be proportional to A. Just behind midrapidity, η=3.0, where the pseudorapidity distributions for the heavy targets peak in central collisions $\alpha \approx 0.3$. This value indicates a dependence on target thickness, which goes as $A^{1/3}$.

Only at midrapidity and in the extreme backward direction does VENUS show the same target dependence as the experimental data.

4.4 Transverse Energy per Charged Particle

The calorimeter MIRAC and the streamer tube detectors have a spatial overlap in the region $2.4 < \eta < 4.0$. They cover the full azimuthal angle in this region. The transverse energy measured by MIRAC and the charged particle multiplicity have been used to extract the transverse energy per charged particle, $<E_T>/<n_{ch}>$. It has been calculated both as a function of centrality through the energy measured by the ZDC and as a function of pseudorapidity in the common angular region. The $<E_T>/<n_{ch}>$ is shown for ^{32}S+Au and Al as a function of pseudorapidity in figure 10 and as a function of E_{ZDC}/E_{beam} in figure 11. The VENUS $<E_T>/<n_{ch}>$ is shown as the solid lines. The results for Ag and Cu lie between the results for Au and Al. For Al there is no centrality dependence of the $<E_T>/<n_{ch}>$. Therefore the data for central and peripheral collisions have been added. The central collisions for ^{32}S+Au are defined by $0.0 < E_{ZDC}/E_{beam} < 0.4$ and the peripheral by $0.4 < E_{ZDC}/E_{beam} < 0.85$.

The $<E_T>/<n_{ch}>$ has large systematic errors since the transverse energy density and the charged particle density each have systematic errors of 5–10%. The error bars of figure 10 for central ^{32}S+Au collisions show the part of the systematic error that would influence the shape of the distribution. In addition there is an uncertainty of 5–10% in the absolute levels. For ^{32}S+Al and peripheral ^{32}S+Au data the systematic error is about half of what is indicated for the central ^{32}S+Au data. In figure 11 typical systematic errors have been included for three of the data points for ^{32}S+Au in the region $3.2 < \eta < 4.0$. For the other ^{32}S+Au data points the errors are about the same, but for central ^{32}S+Al they are only about 5–6%. Also these values have an uncertainty of 5–10% in the absolute levels. The statistical errors are smaller than the symbols. Although the systematic errors are large it is still possible to draw some conclusions based on the data.

- $<E_T>/<n_{ch}>$ decreases with increasing target mass at midrapidity.

- A centrality dependence exists for the heavy targets in the most forward angular region where the $<E_T>/<n_{ch}>$ decreases with increasing centrality.
- The pseudorapidity dependence of $<E_T>/<n_{ch}>$ increases with target mass.
- $<E_T>/<n_{ch}>$ is rather similar for peripheral collisions with heavy targets to the values for the lightest target.
- VENUS has the same qualitative behaviour as the experimental data. The trends are however stronger in the experiment.

The $<E_T>/<n_{ch}>$ has a pseudorapidity dependence in FRITIOF, but no centrality dependence. It therefore seems as if the centrality dependence is due to rescattering or possibly the protons which in the VENUS model are closer to midrapidity.

HELIOS[13] has found similar dependences on pseudorapidity and centrality as the ones obtained above. In the oxygen data[9] published by WA80 a value of $<E_T>/<n_{ch}>$ of 0.5–0.6 GeV was measured in the region $2.4< \eta <4.0$ for targets of C, Cu, Ag and Au. The higher value was for the peripheral collisions. Adding the two samples obtained for different angular regions of ^{32}S+Au in this analysis gives values of 0.56–0.63 GeV. For the Al target 0.64–0.66 GeV.

5 Discussion

Comparisons between the results of different experiments are difficult to make since the coverage as well as the detectors seldom are identical. A comparison has to be done either through the use of Monte–Carlo models, where all the biases can be simulated or by taking the differences carefully into account. Below some selected multiplicity results of ^{32}S+Au and ^{32}S+W at 200 A GeV are discussed. There is only a 2% difference in the radii of gold and tungsten so the results should be comparable. In conjunction with the comparison the trigger biases of the experiments are studied.

5.1 Charged Particle Densities

The result of this experiment is an average charged particle density of 173 for 2.3% of the hardware minimum bias cross section and 181 for 0.13%. The hardware minimum bias cross section is approximately 3200 mb for ^{32}S+Au in this analysis.

The HELIOS–emulsion collaboration[11] claims to measure densities of up to 178 for ^{32}S+W corresponding to <1% of the total inelastic cross section. According to figure 8 in their article, that value is for an individual bin and the average peak height is around 155–160. They trigger on events with very high transverse energy in the backward region $0.1< \eta <3.0$. At 2% of the inelastic cross section they reach about 140.

HELIOS[13] has shown densities of around 175 taken with a high E_T trigger. Their data were not corrected for decays, γ conversion and hadronic interactions, which would lower the yield. These effects are expected to be important for η <2, but should not exceed 10%. HELIOS has an on–line trigger on transverse energy in two intervals, $-0.1 < \eta < 2.9$ and $-0.1 < \eta < 5.5$. The two triggers produce similar distributions according to HELIOS, which should exclude any significant trigger bias when measuring the E_T in the restricted interval. However their seems to be a small difference. By triggering on high E_T in one region an auto correlation is introduced. Events that happen to have high E_T in that particular region tend to be favoured over those that have high E_T in some other region although the total E_T may be the same. This effect is more severe the smaller the trigger region is.

EMU01[10] gets up to a charged particle density of about 115 with a Au target, but their centrality criterion is not as strong. Their criterion is based on the charge flow at zero degrees. In addition they have a multiplicity cut of at least 300 shower particles. With the same cuts applied to FRITIOF they get as much as 15.9% of the FRITIOF minimum bias cross section, 3860 mb, giving about 610 mb. Their cross sections for ^{16}O+emulsion[5] at 200 A GeV deviated by less than 10% from FRITIOF so the extraction of the above cross section should be reliable. The central cut of E_{ZDC}/E_{beam} <20% in the WA80 experiment can be used for a comparison with the EMU01 results. The cut corresponds to 14.2% of the WA80 minimum bias cross section, which translates into approximately 450 mb. The maximum density of charged particles for this cut is 158.

The emulsion results on pseudorapidity distributions only include shower particles, which are singly charged particles with $\beta > 0.7$. The counter experiments do not make such a distinction. This difference is negligible in the central region where the maximum density is measured. Neutral strange particles like the Λ and the K^0_s are not seen in emulsion. Their lifetime allows them to decay into charged particles before they reach the WA80 multiplicity detectors. For the WA80 data the contribution from these decay products to the yield of charged particles was estimated through FRITIOF to be around 7%. The data have not been corrected for this effect. However it would lower the value of 158 to 147, which can be compared to the EMU01 result of 115. The systematic error of the WA80 measurement is 8–9%. According to EMU01 their systematic error should not exceed 5% and their statistical errors are small. This means that there is a two standard deviation difference between the results. An increase of strangeness production compared to what is expected from FRITIOF could explain part of the difference. The difference in trigger conditions is also important as will be shown in the next section.

The WA80 result of 173 charged particles per pseudorapidity unit for the 2.3% cut of the minimum bias cross section corrected for the 7% neutral strange particle admixture gives 161. This should be compared with the HELIOS–emulsion result of 140 for their 2% cut. Again a lower value is found for the emulsion experiment.

5.2 Trigger Differences

The above results from the HELIOS and the HELIOS–emulsion collaborations have all been taken with a high E_T trigger, whereas WA80 and EMU01 use the energy and charge flow at zero degrees, respectively. To investigate the effect of different kinds of central triggers a simulation of four different central triggers was done with events from FRITIOF. One trigger was in the form of the WA80 zero degree calorimeter. A second trigger was the one used by HELIOS with calorimeters covering $-0.1 < \eta < 5.5$. A third was the charge flow trigger used by emulsion experiments. The number of charged particles in a forward cone with $\theta < 3$ mrad are counted. The fourth trigger was a high multiplicity trigger at midrapidity $2 < \eta < 4$. 30000 minimum bias events ^{32}S+Au were generated. The energy measured at zero degrees, the transverse energy in the region $-0.1 < \eta < 5.5$, the number of charged particles in the forward cone and the multiplicity at midrapidity were calculated for each event. No smearing of the energy with the calorimeter responses was performed. The events were ordered according to centrality for each kind of trigger separately.

In figure 12 the maximum average charged particle density is shown as a function of the fraction of the inelastic cross section for the four ways of ordering the events. The trigger relying on high E_T is above the one depending on low energy flow at zero degrees. For a small projectile nucleus interacting with a large target nucleus as in the case of ^{32}S+Au a large range of impact parameters have all projectile nucleons interacting. The collisions with these small impact parameters all have very little energy going in the forward direction. The zero degree energy signal therefore gets saturated whereas the E_T continues to increase with particle multiplicity. The same behaviour was found when the transverse energy trigger region was chosen as $0.1 < \eta < 3.0$ corresponding to the HELIOS–emulsion coverage. The same procedure was applied for 30000 ^{32}S+Al events. In that case the projectile is slightly larger than the target. The difference between the two triggers was only 2–3% even when going to very small cross sections. For a symmetric system like Pb+Pb you expect the same behaviour as for ^{32}S+Al. It is the relative size of projectile and target that is the relevant quantity with which to explain the trigger difference.

The points for the charge flow trigger are below the ones for the other triggers. The lower densities are explained by two main differences between a charge flow trigger and a calorimeter trigger: 1. A charge flow trigger does not use the information from the neutrals, e.g. the projectile spectator neutrons. 2. All charged particles in the forward cone are equally weighted independent of their energy.

The trigger relying on the multiplicity at midrapidity should be the most effective high charged particle density trigger due to the obvious auto correlation. It is included for comparison with the three other indirect triggers as the close to ultimate trigger for selection of high charged particle densities. Triggers that have an auto correlation to the measured quantity select events with large fluctuations of the triggered quantity. When studying the fluctuations rather than

events with large fluctuations it is better to use an indirect trigger which does not affect the measured quantity directly. The trigger giving the highest yield is not automatically the "best" trigger. The conclusions are that for asymmetric collisions:

- At a fixed portion of the inelastic cross section a high E_T trigger is close to the optimum trigger in selecting events with high charged particle density.
- A zero degree energy trigger and a charge flow trigger give lower charged particle densities than a transverse energy trigger.
- The relative difference between the particle densities obtained with different triggers increase with decreasing fraction of the cross section.

From figure12 HELIOS and the HELIOS–emulsion results should lie 5–6% above the WA80 results for the same fraction of very central events. The EMU01 results should lie 5–6% below at 15% of the inelastic cross section. The contribution from the neutral strange particles of course has to be corrected for first.

5.3 Widths

The widths of the pseudorapidity distributions at 200 A GeV measured in emulsion experiments have a standard deviation of 1.3–1.5[11, 25, 26]. The dependence on both projectile and target mass as well as centrality is weak. The widths measured by WA80, as shown in figure 8, exhibit a stronger dependence on centrality and a systematic difference between targets. Such an effect was seen already in the oxygen data at 200 A GeV by Åkesson et al[7].

The emulsion experiments only include shower particles, whereas all charged particles are included in the data presented here. This difference might explain the apparent disagreement. As was explained in an earlier section the relative contribution to the yield of particles from fragmentation of target and projectile is higher for peripheral collisions than for central collisions. The fragmentation products end up at low and high pseudorapidity and give a broader distribution if they are included. The importance of target fragmentation increases with increasing target mass giving wider distributions. When models that do not include target fragmentation are compared to the emulsion data they are able to reproduce the widths nicely[10, 11, 12]. For central collisions where the relative contribution from fragmentation to the yield of charged particles is small the widths of this experiment are 1.3–1.4 with a typical systematic error of 0.1. The width in the WA80 transverse energy measurements for central collisions was 1.4±0.1[23]. For central collisions the width is basically governed by the energy of the projectile[27].

6 Conclusions

Measured pseudorapidity densities of ^{32}S+Au reach 170–180 charged particles per pseudorapidity unit. The density is in agreement with electronically measured

HELIOS results, but is above EMU01 and HELIOS–emulsion data even when different experimental biases are taken into account. VENUS densities are somewhat above the WA80 data. The general agreement between the WA80 data and VENUS is fair, but in the backward region the data show a higher yield for the heavy targets.

The large widths of the pseudorapidity distributions in peripheral collisions are attributed to target fragmentation.

The yield of charged particles in the target region is directly proportional to the target mass for central collisions of ^{32}S on heavy targets. A weaker dependence was seen for ^{16}O at the same bombarding energy per nucleon and for the same targets.

The transverse energy per charged particle varies as a function of pseudorapidity in the interval $2.4 < \eta < 4.0$. For the heavy targets there is also a centrality dependence .

The trigger influence on the measurement of charged particle densities was studied in a Monte–Carlo simulation. A trigger relying on high transverse energy around midrapidity is better in selecting high charged particle density events than a trigger based on the absence of energy or charge at zero degrees.

7 Acknowledgements

We thank the accelerator divisions of CERN, GSI and LBL for their excellent work, which has led to the development and delivery of the ^{32}S beams. The partial support by the German BMFT and DFG, the United States DOE, the Swedish NFR and the Humbolt Foundation is gratefully acknowledged.

References

[1] Proceedings of the QUARK MATTER '90 conference in Menton, France, Nucl. Phys **A525**(1991).

[2] J.D. Bjorken, Phys. Rev. D. **27**(1983)140.

[3] E802–collaboration, P. Vincent et al., Nucl. Phys **A498**(1988)67c.

[4] E814–collaboration, J. Barette et al., submitted to Phys. Rev. C.

[5] EMU01–collaboration, M.I. Adamovich et al., Phys. Rev. Lett. **62**(1989)2801.

[6] L.M. Barbier et al., Phys. Rev. Lett. **60**(1988)405.

[7] HELIOS–collaboration, T. Åkesson et al., Nucl. Phys. **B333**(1990)48.

[8] NA35–collaboration, A. Bamberger et al., Phys. Lett. **184B**(1988)583.

[9] WA80–collaboration, R. Albrecht et al., Phys. Lett. **202B**(1988)596.

[10] EMU01–collaboration, M.I. Adamovich et al., Phys. Lett. **227B**(1989)285.

[11] HELIOS–Emulsion–collaboration, T. Åkesson et al., Nucl. Phys. **B342**(1990)279.

[12] P.L. Jain, K. Sengupta, G. Singh and A.Z.M. Ismail, Phys. Lett. **235B**(1990)351.

[13] HELIOS–collaboration, L. Ramello et al., Nucl. Phys. **A498**(1989)403c.

[14] HELIOS–collaboration, L. Ramello et al., Nucl. Phys. **A525**(1991)555c.

[15] WA80–collaboration, R. Albrecht et al., GSI–report GSI-85-32(1985).

[16] K. Werner and P. Koch, Phys. Lett. **242B**(1990)251.

[17] A. Baden et al., Nucl. Inst. Meth. **A203**(1982)189.

[18] R. Albrecht et al., Nucl. Inst. Meth. **A276**(1989)131.

[19] G.R. Young et al., Nucl. Inst. Meth. **A279**(1989)503.

[20] T. C. Awes et al., Nucl. Inst. Meth. **A279**(1989)479.

[21] E. Albini et al., Nuovo Cimento **32A**(1976)101.

[22] WA80–collaboration, R. Albrecht et al., Z. Phys. **C45**(1989)31.

[23] WA80–collaboration, R. Albrecht et al., Phys. Rev. **C44**(1991)2736.

[24] B. Nilsson–Almqvist and E. Stenlund, Comp. Phys. Comm. **43**(1987)387.

[25] H. von Gersdorff et al., Phys. Rev. **C39**(1989)1385.

[26] EMU01–collaboration, M.I. Adamovich et al., to be submitted to Phys. Rev. Lett.

[27] J. Stachel, Nucl. Phys. **A525**(1991)23c.

Figure 1: Minimum bias multiplicity distributions of charged particles, n_{ch}, in ^{32}S + Al, Cu, Ag and Au interactions. The interval covered is -1.7< η <4.0. The VENUS results are indicated by the solid lines.

Figure 2: Pseudorapidity distribution of charged particles for ^{32}S + Al collisions for three different centrality cuts, 0–35%, 45–55% and 75–85% of the beam energy measured at zero degrees. The VENUS results are indicated by the solid lines.

Figure 3: Pseudorapidity distribution of charged particles for ^{32}S + Cu collisions for three different centrality cuts, 0–20%, 45–55% and 75–85% of the beam energy measured at zero degrees. The VENUS results are indicated by the solid lines.

Figure 4: Pseudorapidity distribution of charged particles for ^{32}S + Ag collisions for three different centrality cuts, 0–20%, 45–55% and 75–85% of the beam energy measured at zero degrees. The VENUS results are indicated by the solid lines.

Figure 5: Pseudorapidity distribution of charged particles for ^{32}S + Au collisions for three different centrality cuts, 0–20%, 45–55% and 75–85% of the beam energy measured at zero degrees. The VENUS results are indicated by the solid lines.

Figure 6: Maximum charged particle density, ρ_{max}, of a Gaussian fit to the pseudorapidity distributions as a function of E_{ZDC}/E_{beam} for ^{32}S+Al, Cu, Ag and Au. The VENUS results are indicated by the solid lines.

Figure 7: Peak position, η_{peak}, of a Gaussian fit to the pseudorapidity distributions as a function of E_{ZDC}/E_{beam} for ^{32}S+Al, Cu, Ag and Au. The VENUS results are indicated by the solid lines.

Figure 8: Width, σ, of a Gaussian fit to the pseudorapidity distributions as a function of E_{ZDC}/E_{beam} for ^{32}S+Al, Cu, Ag and Au. The VENUS results are indicated by the solid lines.

Figure 9: Target mass dependence, α, on the yield of charged particles as a function of η. The mass dependence was parameterized as $\Delta n_{ch}/\Delta\eta \sim A^{\alpha}$. A is the target mass number. The VENUS result is indicated by the solid line.

Figure 10: $<E_T>/<n_{ch}>$ for ^{32}S+Au and Al as a function of pseudorapidity. The Au data have been split up into two samples, one central and one peripheral. The VENUS results are indicated by the solid lines. They are from the top, Al, Au peripheral and Au central. The systematic errors have been included for central ^{32}S+Au collisions only. For the other two samples the systematic errors are lower by a factor of 2. In addition there is a uncertainty of 5–10% in the absolute levels for all three data sets.

Figure 11: $<E_T>/<n_{ch}>$ for ^{32}S+Au and Al as a function of E_{ZDC}/E_{beam} for different pseudorapidity intervals. The VENUS results are indicated by the solid lines. The two short lines are for Al with the top line for the lower pseudorapidity values. The long lines are for Au with the top line for the lower pseudorapidity values. Three typical systematic error have been inserted for the data points for the ^{32}S+Au data in the region $3.2< \eta <4.0$. The errors are similar for the other ^{32}S+Au data, but only 5–6% for the central ^{32}S+Al data. In addition there is a uncertainty of 5–10% in the absolute levels for all four data sets.

Figure 12: Four different triggers are simulated using events from the FRITIOF model. The maximum charged particle density, ρ_{max}, is shown as a function of the fraction of the inelastic cross section for ^{32}S+Au interactions. The different triggers are: a multiplicity trigger in the interval $2< \eta <4$, a transverse energy trigger in the interval $-0.1< \eta <5.5$, a trigger depending on the energy flow at zero degrees ($\eta >6.0$) and a trigger based on the charge flow at zero degrees $\theta <3$ mrad. Only the 20% most central part of the triggers are shown in the figure.

Figure 1

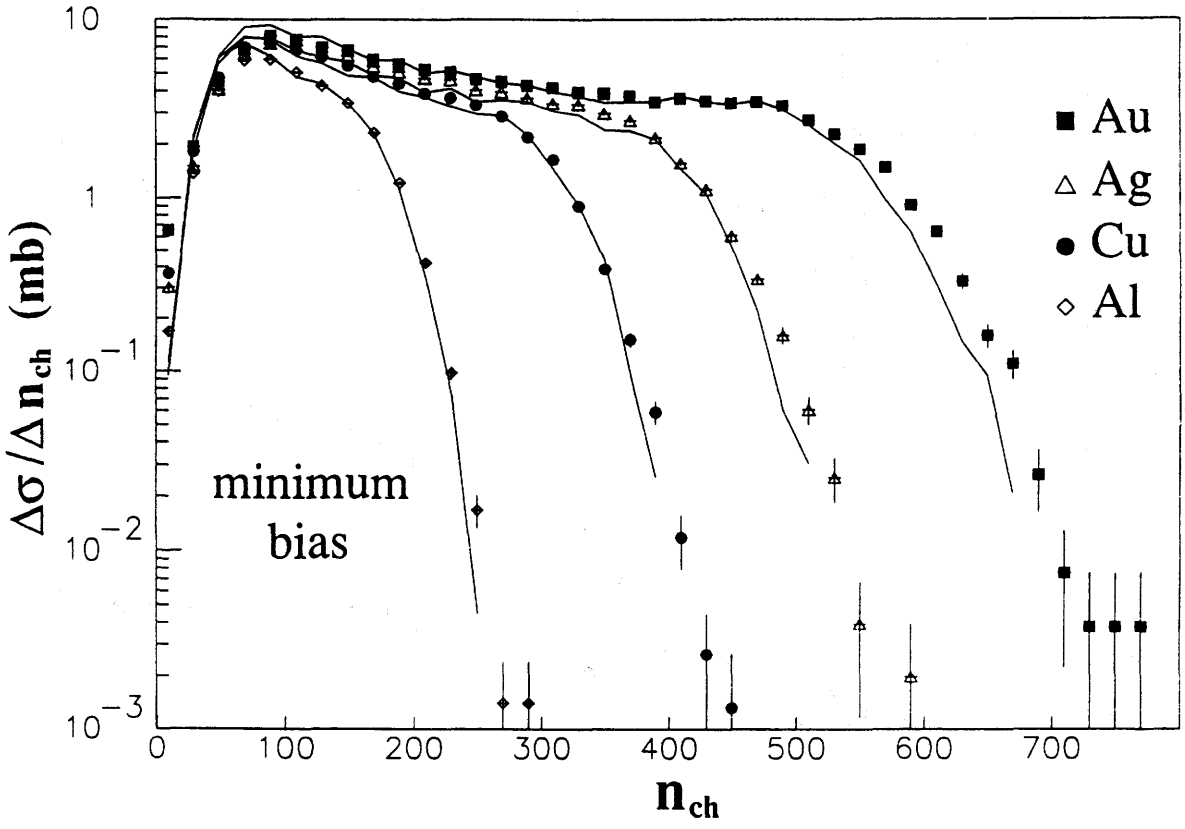

Figure 2

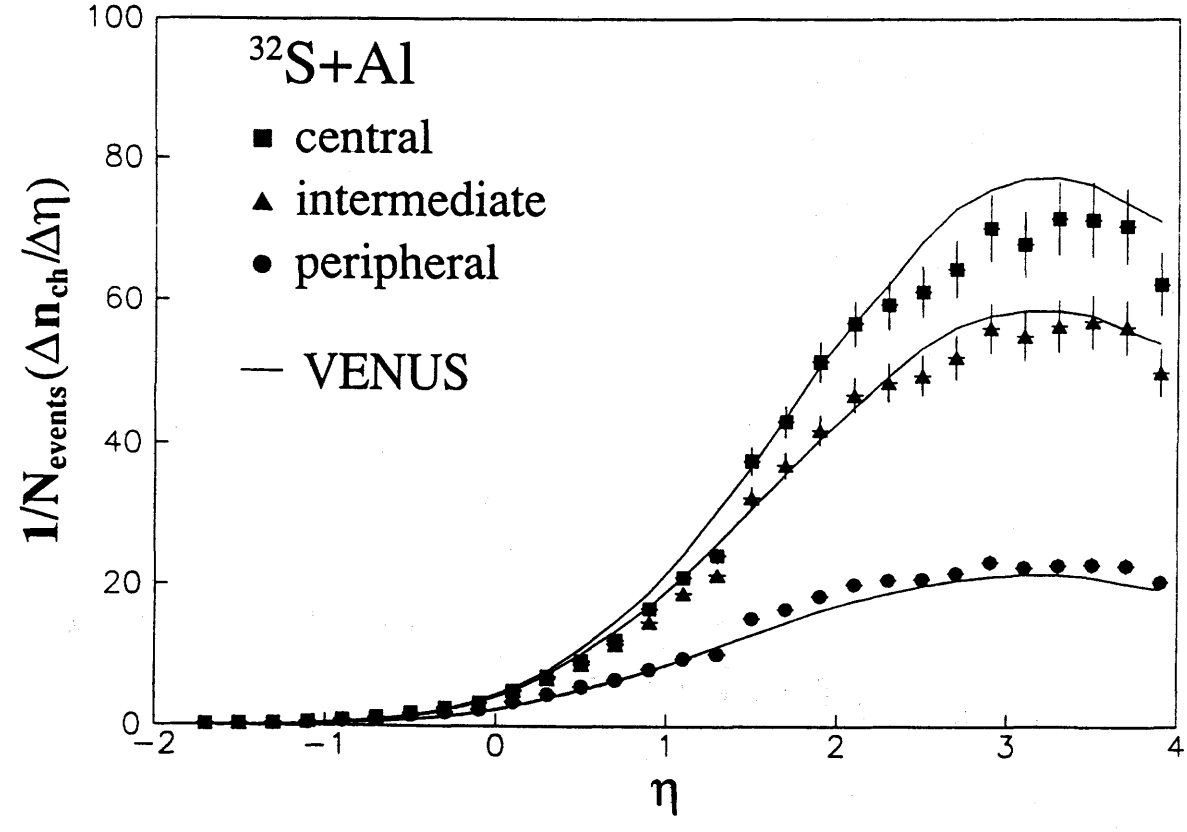

Figure 3

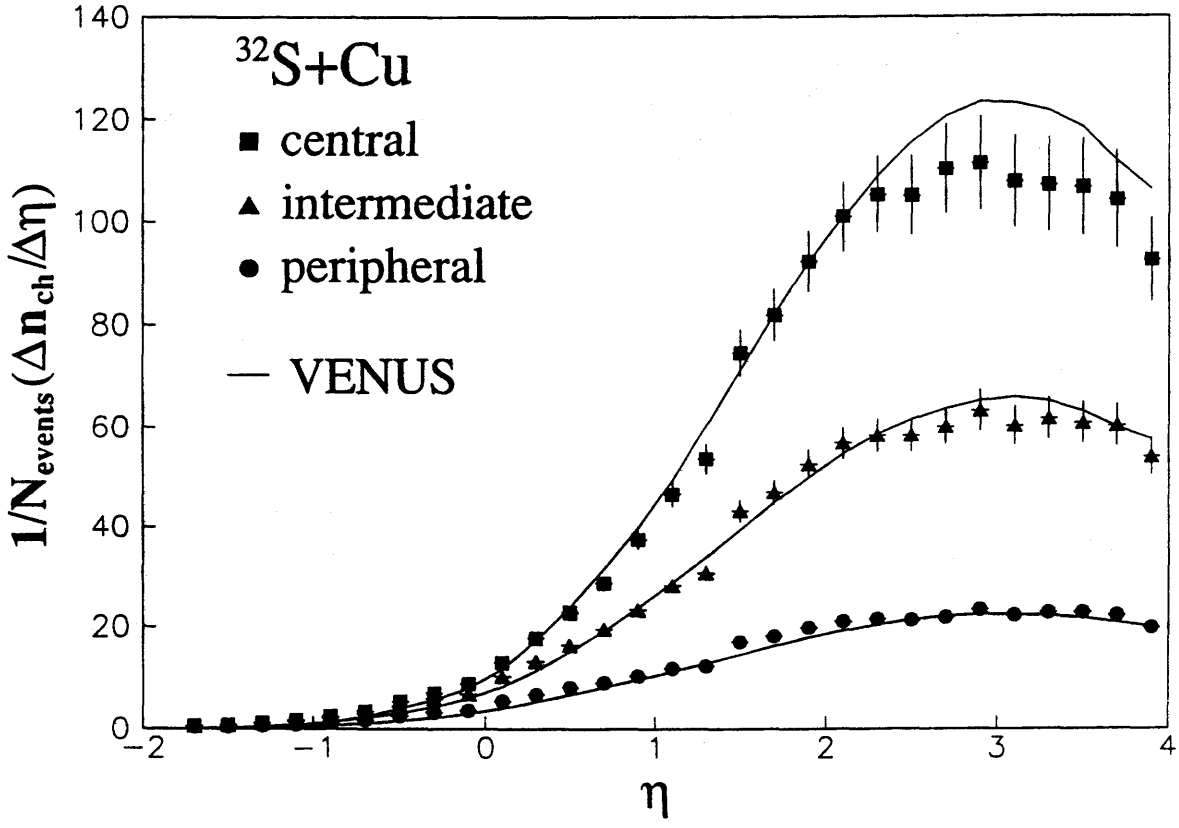

Figure 4

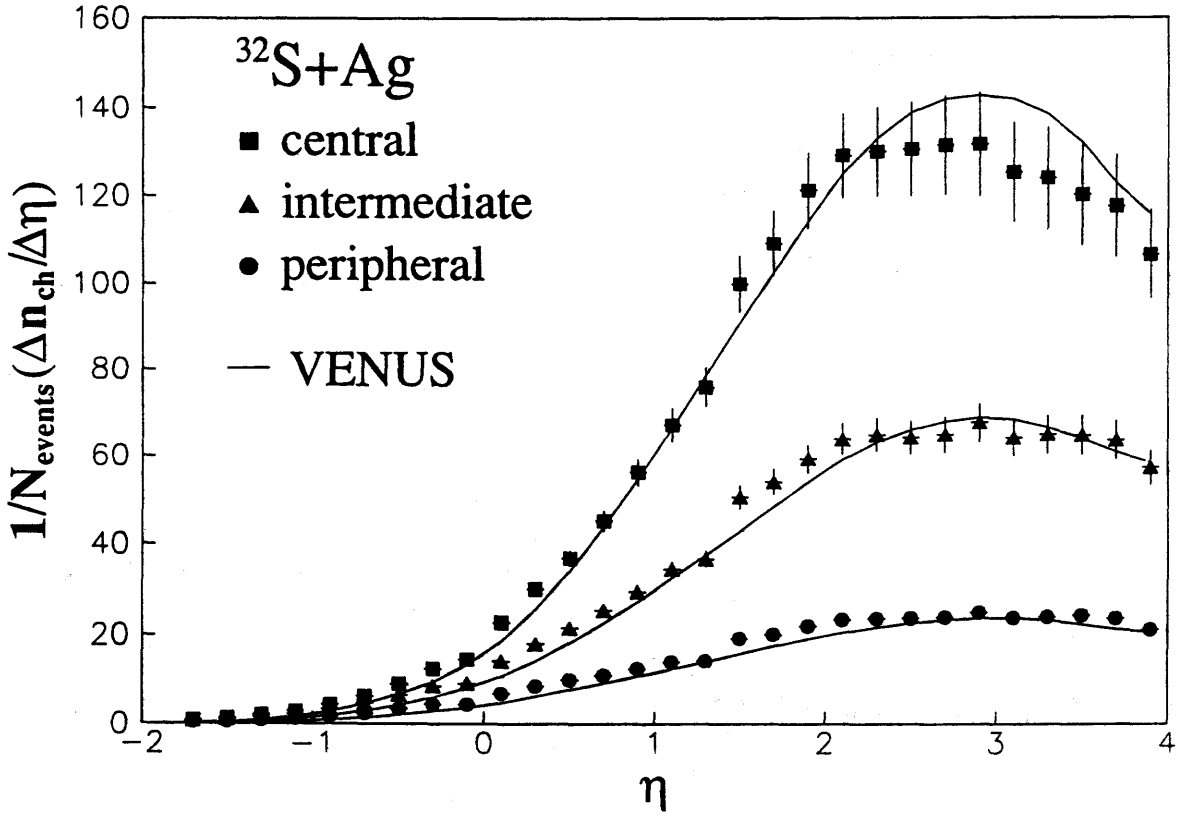

Figure 5

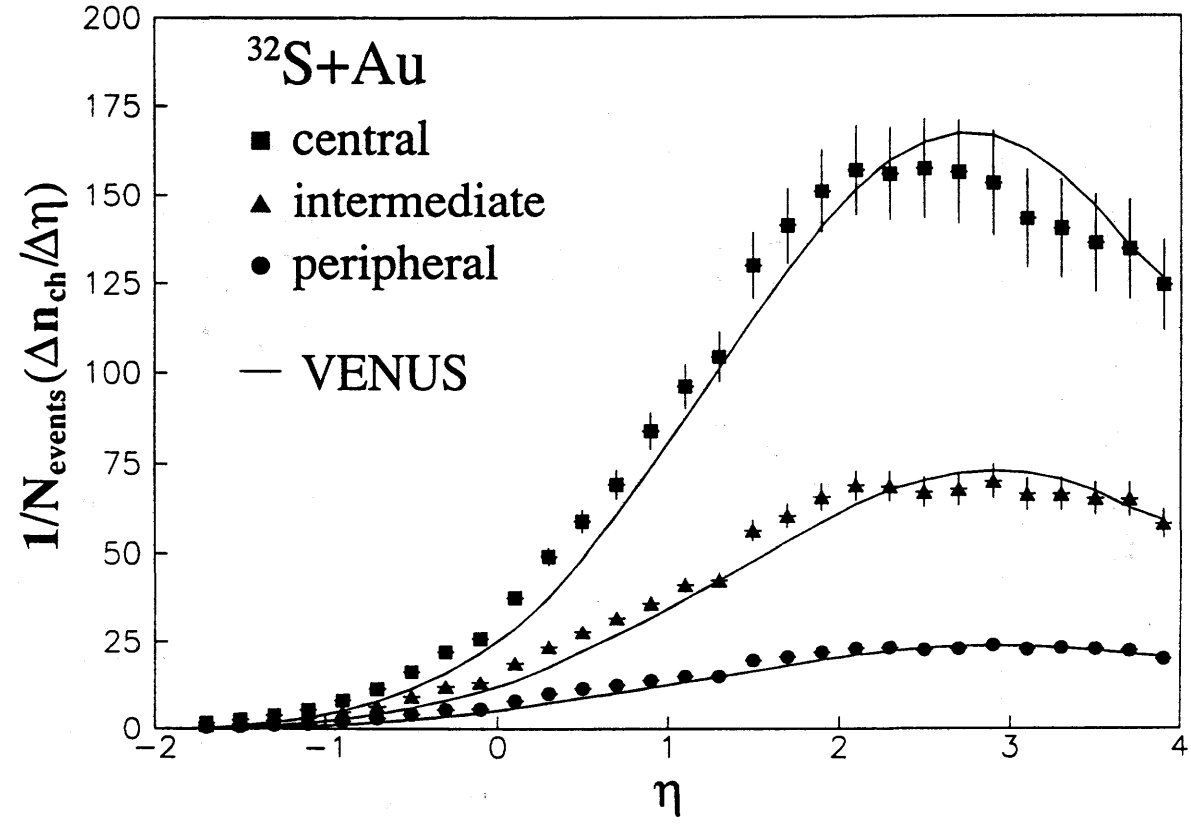

Figure 6

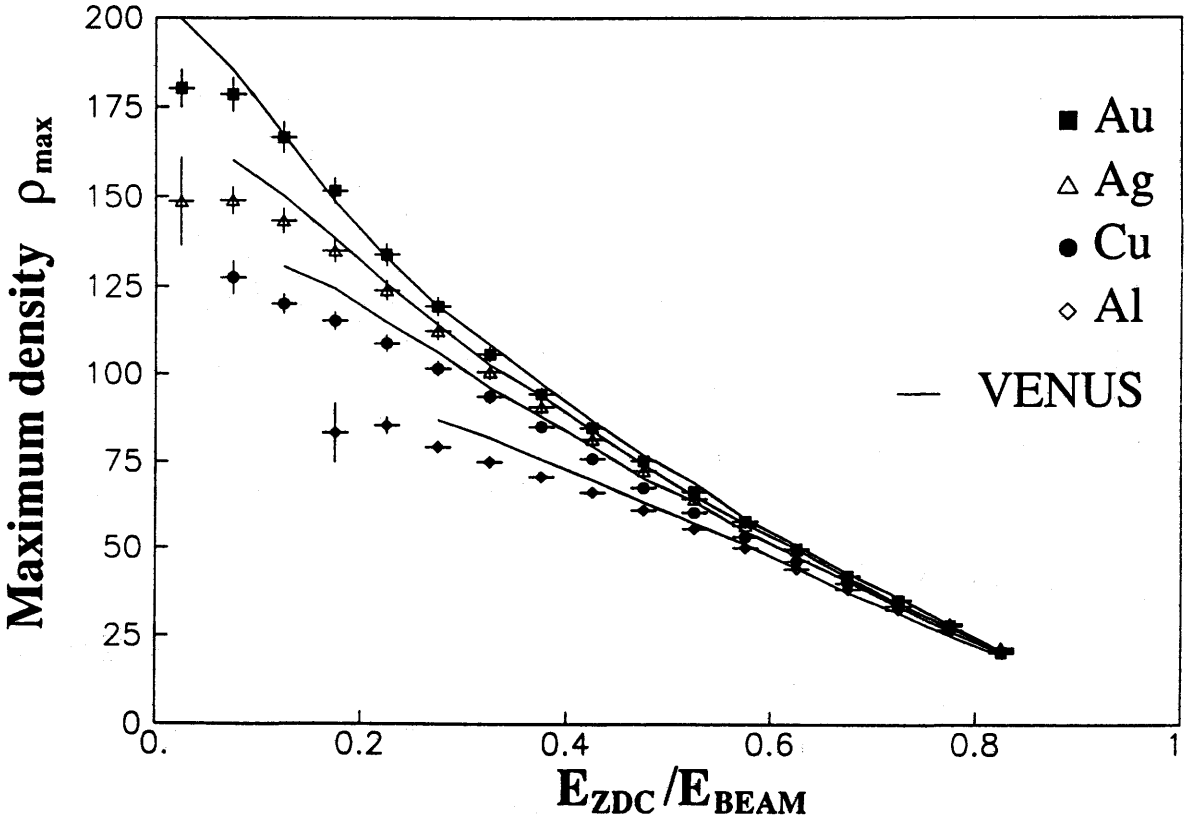

Figure 7

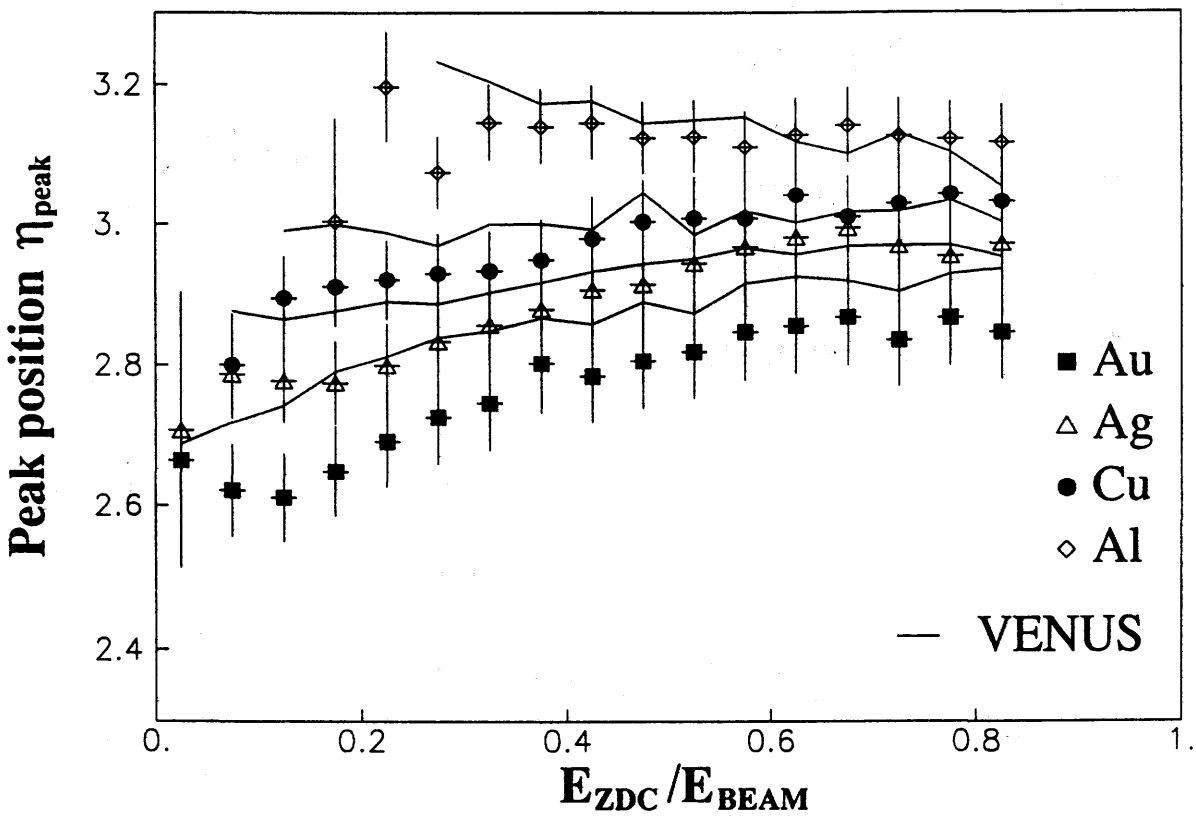

Figure 8

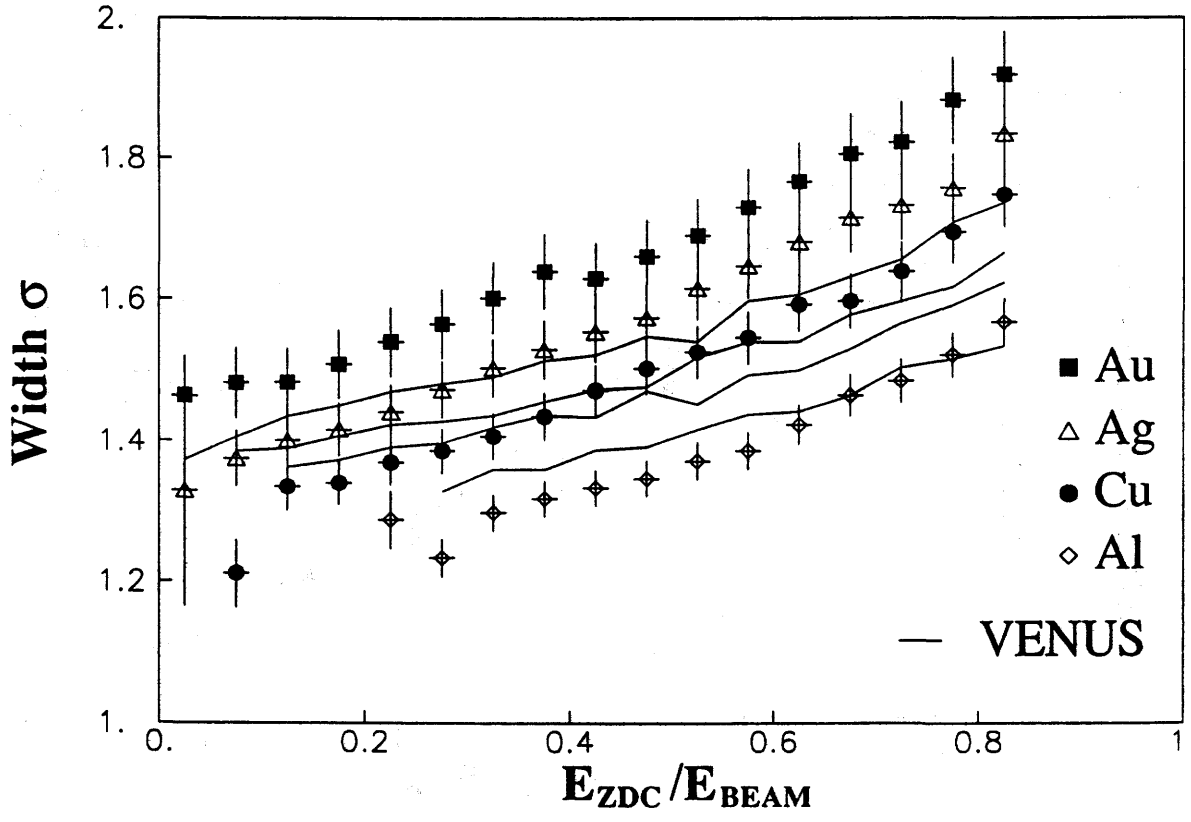

Figure 9

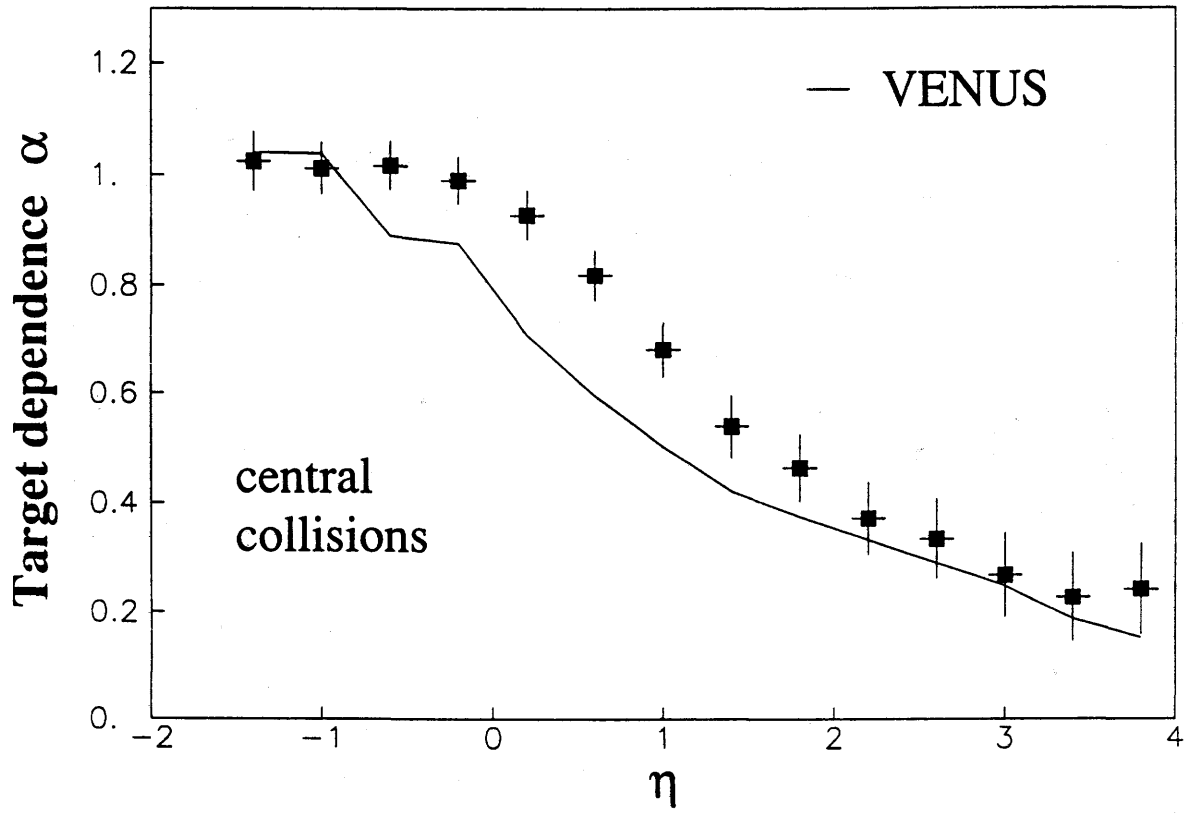

Figure 10

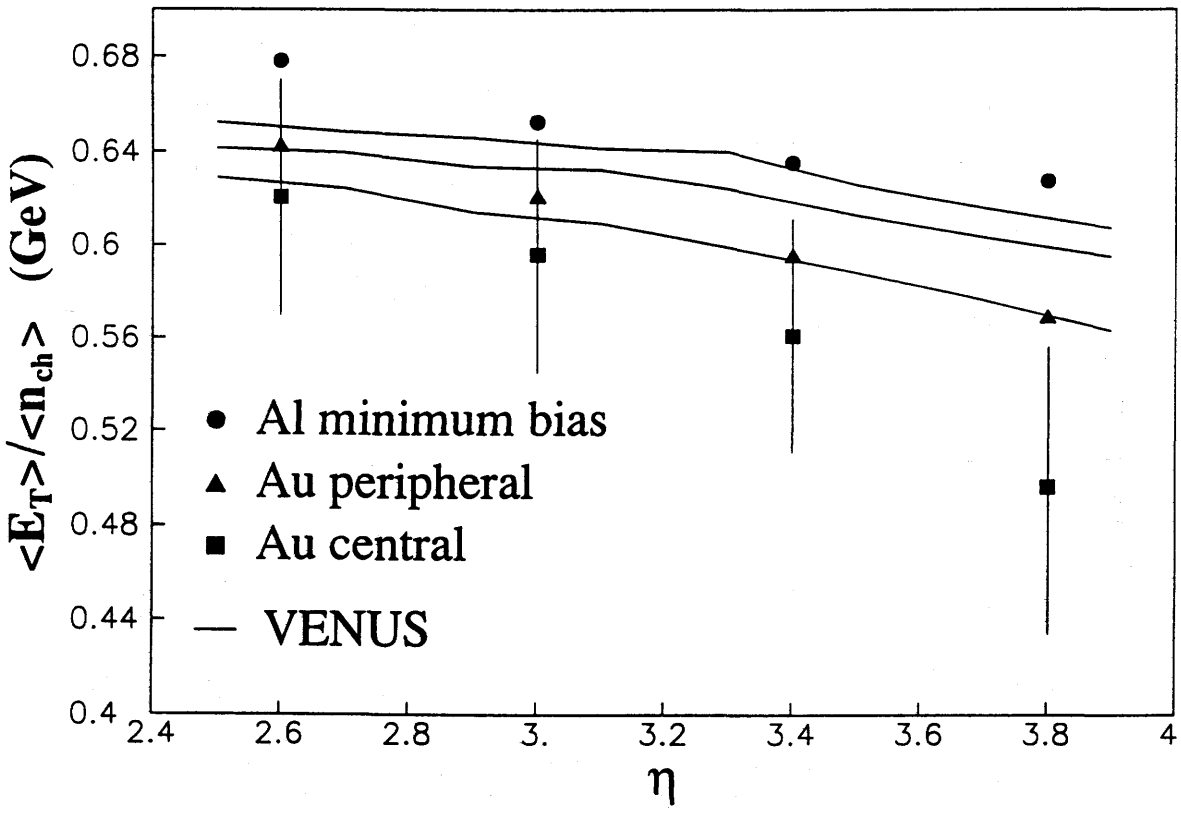

Figure 11

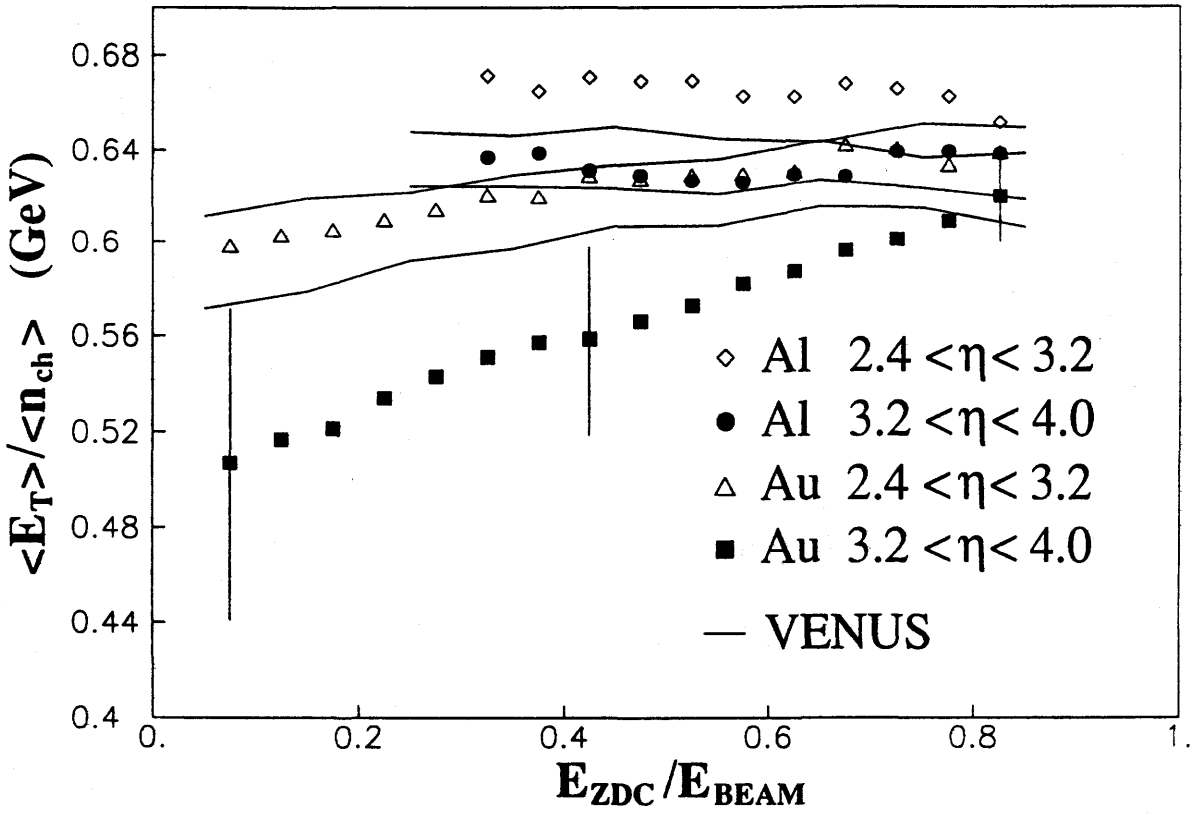

Figure 12